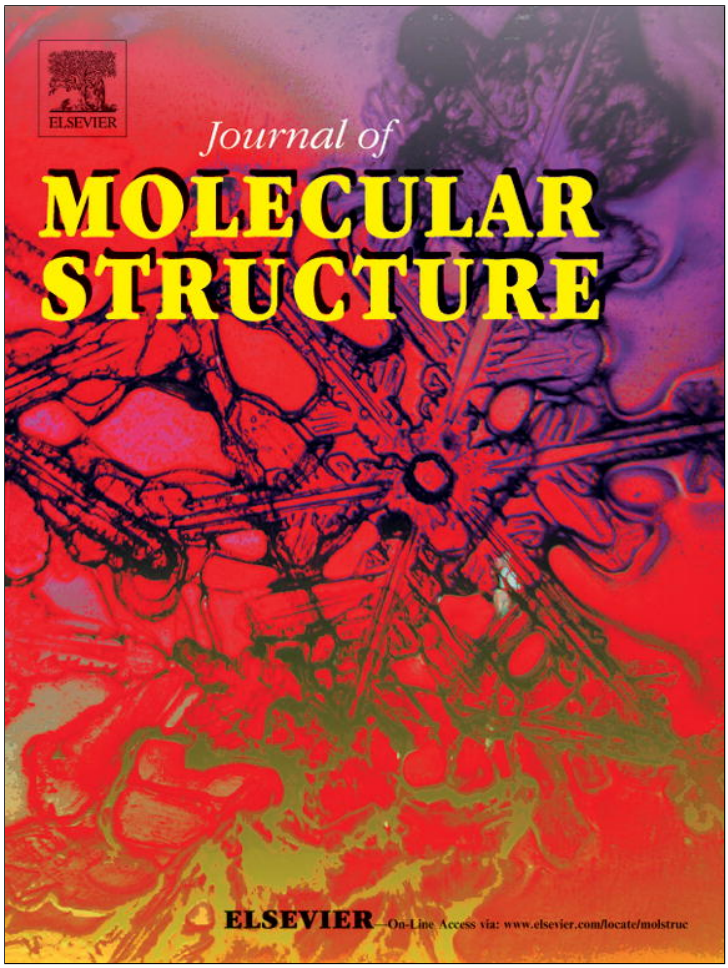

Journal of Molecular Structure 1045 (2013) 180–190

Contents lists available at SciVerse ScienceDirect

Journal of Molecular Structure

journal homepage: www.elsevier.com/locate/molstruc

Single crystal, spectral, computational studies and *in vitro* cytotoxicity of 2-chloro-3-formylpyrido[2,1-a]isoquinoline-1-carbonitrile derivative

Ahmed M. Mansour, Hamdi M. Hassaneen, Yasmin Sh. Mohammed, Nour T. Abdel Ghani *

Chemistry Department, Faculty of Science, Cairo University, Gamaa Street, Giza 12613, Egypt

HIGHLIGHTS

- The unit-cell of PQC is built by two molecules of different conformations.
- DFT/B3LYP gives better agreement than HF method.
- MCF7 cell line is more sensitive to PQC than HCT and HEPG2.
- PQC has several sites for electrophilic attack.
- The inclusion of solvation to NMR calculations is essential for acidic protons.

ARTICLE INFO

Article history:
Received 15 January 2013
Received in revised form 6 April 2013
Accepted 8 April 2013
Available online 24 April 2013

Keywords:
Pyrido[2,1-a]isoquinoline
Crystal structure
Antitumor
NBO
PCM
GIAO

ABSTRACT

In the present work, comprehensive theoretical and experimental structural studies on 2-chloro-3-formyl-9,10-dimethoxy-4-oxo-6,7-dihydro-4H-pyrido[2,1-*a*]isoquinoline-1-carbonitrile (PQC) have been performed using spectral methods and X-ray crystallography. PQC crystallizes in monoclinic crystal system of $P2_1/c$ space group with $a = 23.5106\ (6)$ Å, $b = 17.7940\ (4)$ Å, $c = 7.2843\ (2)$ Å and $\beta = 90.1421\ (9)^\circ$. The unit-cell is built by two molecules of different conformations. The two molecules are not coplanar and they are linked to each other through double intermolecular hydrogen bonds of different strength. Optimized molecular structure and harmonic vibrational frequencies have been investigated at DFT/B3LYP and HF level of theory combined with 6-31G(d) basis set. Stability, arises from hyperconjugative interactions, charge delocalization and H-bond, has been analyzed using natural bond orbital (NBO) analysis. Electronic structures were discussed by time-dependent density functional theory. Descriptions of frontier molecular orbitals and the relocation of the electron density were determined. ^{1}H NMR chemical shifts were computed by using Gauge-invariant atomic orbital method in both gas and DMSO media, using the polarizable continuum model. The cytotoxicity assay was performed against three-cell lines, breast cancer (MCF7), colon Carcinoma (HCT) and human heptacellular Carcinoma (HepG2).

1. Introduction

Quinoline and isoquinoline derivatives are a useful structural motif for displaying chemical functionality in biologically active molecules. Some derivatives have potent biological activities as antibacterial [1] against some gram-positive and gram-negative bacteria. Amino-quinoline derivatives are used as inhibitors of human immuno deficiency virus (HIV) [2]. For example, 4-amino-quinoline was used in treatment of erythrocytic plasmodial infections [3]. Pyrrolizidinylalkyl derivatives of 4-amino-7-chloroquinoline exhibited excellent antimalarial activity [4], through the accumulation in the acidic digestive vacuoles of the malaria parasite. Hence, it inhibits conversion of toxic haematin to β-haematin. Likewise, 8-aminoquinoline constitutes a family of drugs namely, primaquine, tafenoquine and pamaquine [5] that is used in the treatment of malaria. Some isoquinolines exhibited other activities such as anti-filarial [6], anti-neoplastic [7] and as cardiovascular agents [8].

As continuation studies [9–11] on synthesis and characterization of some biologically active compounds and seeking to understanding the role of isoquinoline moiety in the cytotoxicity assay against some cell lines, comprehensive experimental and theoretical studies of PQC (Fig. 1) at density functional theory (DFT) and *ab initio* Hartree Fock (HF) have been carried out. Atomic charges, distribution of electron density (ED) in various bonding and anti-bonding orbitals and stabilization energies, E^2 have been calculated by NBO analysis. The effect of solvent on ^{1}H NMR data was carried by applying the polarizable continuum model. Comparison between experimental and theoretical IR bands was discussed. To understand the electronic transitions, time-dependent density

* Corresponding author. Tel.: +20 2 01006700375; fax: +20 2 35728843.
E-mail address: noureta2002@yahoo.com (N.T. Abdel Ghani).

0022-2860/$ - see front matter © 2013 Elsevier B.V. All rights reserved.
http://dx.doi.org/10.1016/j.molstruc.2013.04.032

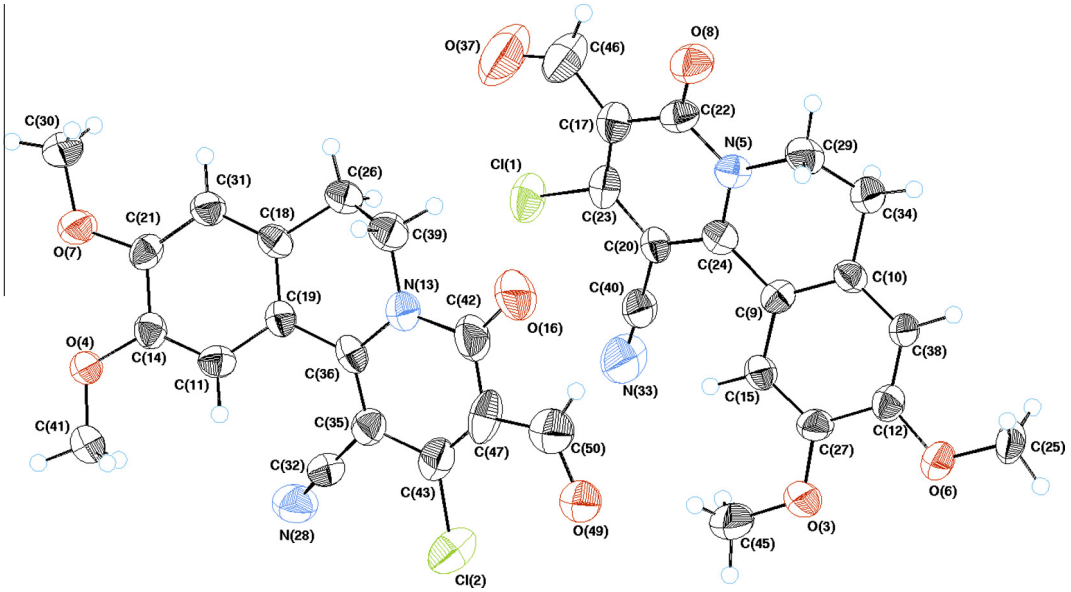

Fig. 1. ORTEP plot of 2-chloro-3-formyl-9,10-dimethoxy-4-oxo-6,7-dihydro-4H-pyrido[2,1-a]isoquinoline-1-carbonitrile.

functional theory (TD-DFT) calculations have been also applied. The reactivity of dimeric and monomeric PQC in terms of global hardness (η), softness (S), electrophilicity index (ω), molecular polarizability (α), Mulliken electronegativity (χ), and molecular electrostatic potential (MEP) has been also discussed.

2. Experimental

2.1. Synthesis and characterization

Isoquinoline-1-acetonitrile [12] **(1)** and 2-hydroxy-9,10-dimethoxy-4-oxo-6,7-dihydro-4*H*-pyrido[2,1-a]isoquinoline-1-carbonitrile **(2)** [13] were prepared according to the procedures reported in the literature. Phosphoryl chloride (70.0 g, 0.46 mol) was added drop wise over a period of 30 min to DMF (12.0 g, 0.24 mol) at 0 °C. To the resulting mixture, compound **(2)** (40.0 g, 0.13 mol) was added and then the reaction mixture was stirred at 60–70 °C for 5 h. After cooling, this reaction mixture was poured into cold H_2O (500 ml) and left for 3 h. The solid product was collected, washed with ethanol and crystallized from DMF to give the studied compound **(3)** [14] (Scheme 1) as orange crystals, mp 262–264 °C (DMF), 85% yield; FT IR (KBr) ν 2214 (C≡N), 1720 (C=O), 1657 (C=O) cm^{-1}; ^{1}H NMR (DMSO) δ 2.98 (m, 2H), 3.84 (s, 3H), 3.91 (s, 3H), 4.11 (m, 2H), 7.15 (s, 1H), 7.89 (s, 1H), 10.14 (s, 1H) ppm; MS, *m/z* (%): 345 (M^+ + 2, 9.9), 344 (M^+, 23.4), 316 (100.0), 301 (77.4). Anal. Calcd for $C_{17}H_{13}ClN_2O4$: C, 59.23; H, 3.80; Cl, 10.28; N, 8.13. Found: C, 59.10; H, 3.60; Cl, 10.41; N, 7.91. The mass spectrum of the titled compound shows a molecular ion peak at *m/z* 344 with a fragmentation pattern as shown in Scheme (S1) (Supplementary material).

2.2. Physical measurements

FT IR spectrum was recorded as KBr pellet using *FT IR-460 plus, JASCO*. EIMS was obtained from *SHIMADZU QP-2010 plus mass spectrometer* at 70 eV. ^{1}H NMR spectrum was recorded at 300 MHz in DMSO-d_6 using *Varian-Oxford Mercury VX-300 NMR*. Electronic absorption spectra were obtained by UV–Vis. *SHIMADZU Lambda 4B* automated spectrophotometer. Elemental microanalyses were performed at Micro-analytical Center, Cairo University.

2.3. Crystal structure determination and refinement

The crystallographic analysis was carried out on an *Enraf–Nonius CAD4 diffractometer*, using graphite monochromated Mo Kα radiation (k = 0.71073 Å) at 296 K. Three standard reflections were monitored during data collection and no significant intensity decay was observed. All diffracted intensities were corrected for Lorentz and polarization effects [15–16]. The structure was solved by direct methods and was refined by the full-matrix least-squares method using *SIR*92 [17] computer programs in the space group $P2_1/c$. All diagrams and calculations were performed using maXus [18], while the molecular graphics were given using *ORTEP*. The figures involving hydrogen-bonds and packing were drawn using Mercury [19]. Further relevant crystallographic data are summarized (Supplementary material, Table S1).

2.4. Computational details

Full-unconstrained geometry optimizations of PQC have been performed at DFT(B3LYP) and HF level of theory combined with 6-31G(d) using Gaussian03 package [20]. The starting geometry for computational study was obtained from crystallographic data without any symmetry restriction. The optimized geometries were verified by performing a frequency calculation at the same level of theory. Vibrational modes were analyzed *via* Gaussview software [21]. At this level of theory, the calculated harmonic wavenumbers were found to be higher than the corresponding experimental quantities due to electron correlation approximate treatment, anharmonicity effects and basis set deficiencies [22–23]. Vibrational frequencies are scaled as 0.958 for B3LYP/6-31G(d) for the range of wavenumbers above 1700 cm^{-1} and 0.983 for those below 1700 cm^{-1} [24], as well as 0.9067 for HF/6-31G(d). The NMR chemical shifts were computed by B3LYP/6-311 + G(2d,p) method in the gaseous state by applying GIAO approach [25] and the values for the ^{1}H isotropic were referenced to TMS, which was calculated at the same level of theory. The effect of solvent (DMSO) on the theoretical NMR parameters was performed using the default PCM model. NBO analysis [26] was performed using NBO 3.1 program as implemented in the Gaussian03 package at the DFT/B3LYP level. Electronic spectra were obtained by TD-DFT method [27]. Frontier molecular orbitals (FMOs) and MEP were performed by DFT/B3LYP.

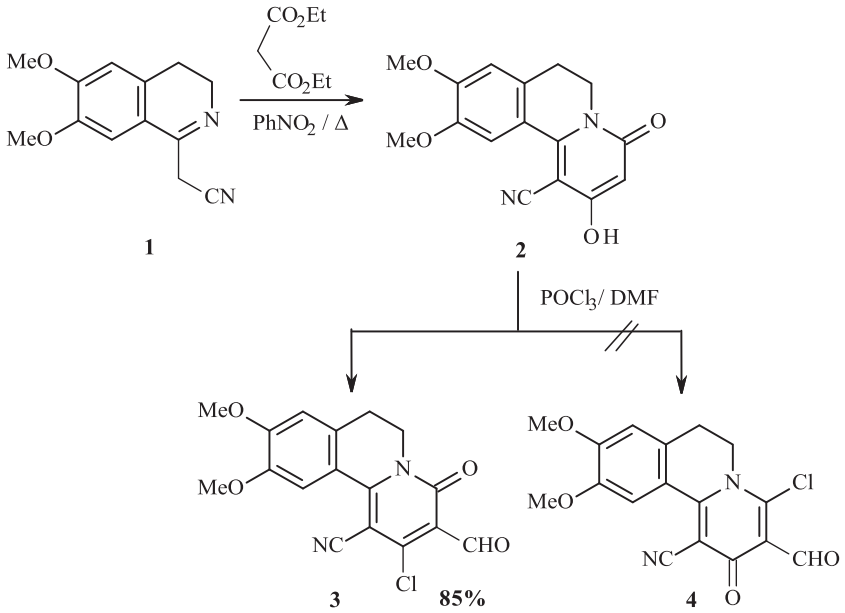

Scheme 1. Synthesis of PQC (3).

Table 1
Selected experimental and calculated bond lengths for the dimeric and monomeric PQC.

Experimental bond length (Å)				Theoretical bond length (Å)				
				Dimer DFT/B3LYP/6-31G(d)		Dimer HF/6-31G(d)		Monomer HF/6-31G(d)
Molecule A		Molecule B		Molecule A	Molecule B	Molecule A	Molecule B	
C9C10	1.385 (4)	C18C19	1.395 (5)	1.405	1.407	1.382	1.382	1.382
C10C38	1.377 (4)	C18C31	1.384 (4)	1.396	1.396	1.391	1.392	1.392
C12C38	1.364 (5)	C21C31	1.375 (4)	1.395	1.395	1.379	1.378	1.378
C12C27	1.414 (4)	C14C21	1.419 (5)	1.424	1.422	1.414	1.414	1.414
C15C27	1.371 (4)	C11C14	1.368 (4)	1.387	1.385	1.369	1.368	1.368
C9C15	1.416 (4)	C11C19	1.398 (4)	1.414	1.414	1.407	1.408	1.407
O3C27	1.368 (4)	O7C21	1.357 (4)	1.350	1.349	1.338	1.332	1.341
O3C45	1.411 (5)	O7C30	1.425 (4)	1.431	1.422	1.408	1.402	1.403
O6C12	1.379 (4)	O4C14	1.351 (4)	1.350	1.355	1.332	1.342	1.332
O6C25	1.429 (4)	O4C41	1.386 (4)	1.421	1.424	1.401	1.403	1.402
C9C24	1.498 (4)	C19C36	1.470 (4)	1.471	1.472	1.479	1.481	1.482
C10C34	1.506 (5)	C18C26	1.496 (5)	1.506	1.504	1.504	1.503	1.504
C29C34	1.520 (5)	C26C39	1.523 (5)	1.520	1.518	1.516	1.514	1.515
N5C24	1.374 (4)	N13C36	1.367 (4)	1.367	1.367	1.356	1.477	1.357
N5C29	1.487 (4)	N13C39	1.481 (4)	1.480	1.478	1.474	1.477	1.473
N5C22	1.394 (4)	N13C42	1.419 (5)	1.423	1.426	1.398	1.396	1.398
C17C22	1.426 (5)	C42C47	1.459 (6)	1.456	1.456	1.456	1.455	1.456
C17C23	1.393 (5)	C43C47	1.348 (5)	1.379	1.380	1.356	1.358	1.355
C20C23	1.393 (4)	C35C43	1.393 (4)	1.425	1.426	1.430	1.430	1.435
O8C22	1.224 (4)	O16C42	1.224 (4)	1.227	1.228	1.202	1.204	1.202
C17C46	1.468 (5)	C47C50	1.434 (4)	1.478	1.478	1.484	1.484	1.490
O37C46	1.193 (5)	O49C50	1.3731	1.220	1.221	1.193	1.192	1.189
Cl 1C23	1.718 (3)	Cl 2C43	1.701 (4)	1.735	1.740	1.721	1.717	1.717
C20C40	1.405 (5)	C32C35	1.435 (5)	1.427	1.426	1.435	1.435	1.435
N33C40	1.148 (5)	N28C32	1.137 (4)	1.164	1.164	1.136	1.136	1.136

2.5. Anticancer activity

Three human cancer cell lines were used for *in vitro* screening experiments; *breast cancer* (MCF7), *colon Carcinoma* (HCT) and *human Heptaocellular Carcinoma* ($HepG_2$). They were obtained frozen in liquid nitrogen (−180 °C) from the American Type Culture Collection. The tumor cell lines were maintained in the National Cancer Institute, Cairo, Egypt, by serial sub-culturing. Potential cytotoxicity of the compounds was tested using Skehan et al. method [28]. Cells were plated in 96-multiwell plate (5×10^3–4×10^4 cells/well) for 24 h before treatment with the compounds to allow the attachment of cell to the wall of the plate. RPMI-1640 medium (5% fetal bovine serum and 2 mM L-glutamine) was used for culturing and maintenance of the human tumor cell lines [29]. Different concentrations of the compound under study were added to the cell monolayer triplicate wells were prepared for each individual dose. The monolayer cells were incubated with the compounds for 48 h at 37 °C and in 5% CO_2 atmosphere. After 48 h, cells were fixed, washed, and stained with the protein-binding dye sulforhodamine B (SRB) [28]. Excess stain was washed with acetic acid and attached stain was recovered with tris-EDTA buffer. The optical density (OD) of each well was measured spectrophotometrically at 564 nm with an ELISA microplate reader and the mean background absorbance was automatically subtracted and

Table 2
Selected experimental and calculated bond angles for the dimeric and monomeric PQC.

Experimental bond angle (°)				Theoretical bond angle (°)				
				Dimer DFT/B3LYP/6-31G(d)		Dimer HF/6-31G(d)		Monomer HF/6-31G(d)
Molecule A		Molecule B		Molecule A	Molecule B	Molecule A	Molecule B	
C27O3C45	117.5 (3)	C14O4C41	118.8 (3)	117.8	118.0	119.4	119.3	120.1
C12O6C25	116.6 (3)	C21O7C30	119.4 (3)	118.5	118.6	120.1	120.2	119.4
C9C10C38	120.5 (3)	C19C18C31	120.1 (3)	119.7	119.7	119.6	119.6	119.1
C10C38C12	120.8 (3)	C18C31C21	120.4 (3)	121.2	121.1	121.0	120.9	121.1
C27C12C38	119.9 (3)	C14C21C31	120.4 (3)	119.2	119.4	119.4	119.5	119.3
C12C27C15	119.7 (3)	C11C14C21	118.4 (3)	119.3	119.1	119.3	119.2	119.3
C9C15C27	120.1 (3)	C14C11C19	121.7 (3)	121.2	121.2	121.1	120.9	121.0
C10C9C15	119.0 (3)	C11C19C18	119.0 (3)	118.9	119.0	119.2	119.5	119.8
C10C34C29	110.1 (3)	C18C26C39	110.2 (3)	108.3	108.3	108.0	107.9	108.0
N5C24C9	116.6 (3)	N13C36C19	116.6 (3)	117.4	117.3	116.9	116.7	116.7
N5C29C34	110.9 (3)	N13C39C26	109.4 (3)	109.8	109.8	109.6	109.6	109.6
C24N5C29	121.5 (3)	C36N13C39	121.5 (3)	119.9	119.8	120.0	120.1	120.1
C22N5C24	122.9 (3)	C36N13C42	123.8 (3)	115.5	124.4	123.8	123.7	123.8
N5C22C17	118.0 (3)	N13C42C47	115.0 (3)	116.3	116.5	116.9	117.1	117.1
C22C17C23	117.6 (3)	C42C47C43	122.0 (3)	118.9	119.0	118.7	118.8	118.7
C17C23C20	122.4 (3)	C35C43C47	119.8 (4)	122.1	121.9	121.7	121.4	121.5
C23C20C24	119.5 (3)	C36C35C43	119.6 (3)	119.3	119.5	119.1	119.4	119.4
N5C22O8	118.6 (3)	N13C42O16	119.5 (4)	119.1	119.2	119.6	119.7	119.4
O8C22C17	123.3 (3)	O16C42C47	125.5 (4)	124.4	124.2	123.4	123.1	123.4
C17C46O37	126.4 (5)	C47C50O49	120.5 (2)	126.2	126.5	126.0	126.2	125.7
Cl 1C23C17	120.1 (3)	Cl 2C43C47	122.6 (3)	121.1	121.1	121.7	121.6	121.8
C20C40N33	177.3 (4)	N28C32C35	176.5 (4)	178.4	178.8	178.2	178.9	179.0

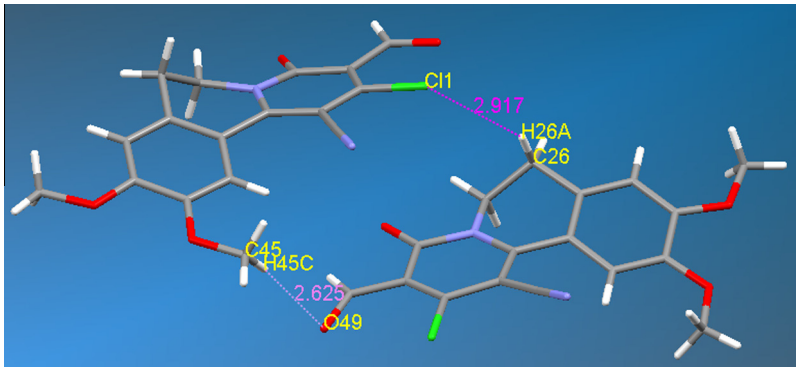

Fig. 2. Hydrogen bond structure of PQC.

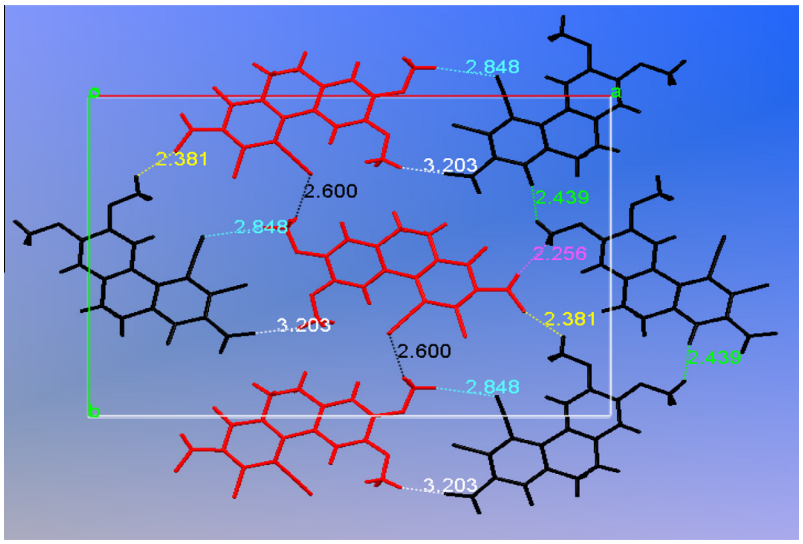

Fig. 3. Intermolecular hydrogen bonding stabilizing the crystal packing of PQC (red (A) and black (B)). (For interpretation of the references to colour in this figure legend, the reader is referred to the web version of this article.)

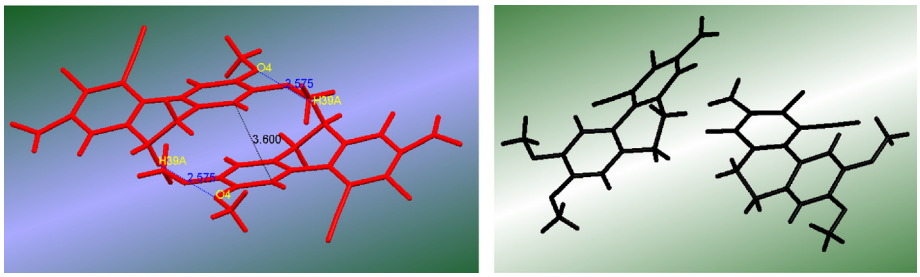

(a) A-type (b) B-type

Fig. 4. A view along "*a*"-axis showing the π–π stacking interactions only in case of "A" type molecules of PQC.

mean values of each drug concentration was calculated. The relation between surviving fraction and drug concentration is plotted to get the survival curve. The results were compared with a similar run of Doxorubicin as an antitumor compound.

3. Results and discussion

3.1. X-ray crystallography

A view of the molecular structure of PQC is shown in Fig. 1. Selected crystallographic data are presented in Tables 1 and 2. PQC crystallizes in monoclinic crystal system of $P2_1/c$ space group with $a = 23.5106\ (6)$ Å, $b = 17.7940\ (4)$ Å, $c = 7.2843\ (2)$ Å [14]. The unit-cell is built by two molecules, $2\cdot[C_{17}H_{13}ClN_2O_4]$, of different conformations. As shown in Fig. 2, the two molecules are not coplanar. They are linked to each other through two intermolecular hydrogen bonds of different strength. Two types of hydrogen bond were known [27]. The most common is the conventional H-bond, defined as A—H···B where A and B are electronegative atoms as N, O or X. The other type is C—H···B, where B is either an electronegative atom carrying one or more electron lone pairs or a region of excess electron density (π electrons of an aromatic system) [27]. Herein, the first H-bond is CH═O49···H—CH_2O45 with a distance of 2.625 Å. The second one is Cl 1···H—C26—H with a distance of 2.917 Å. It is well-known that linear H-bonds are usually stronger than the bonds where the X—H···Y angle is deviated from the linearity [11]. Hence, CH═O49···H—CH_2O45 is stronger than Cl 1···H—C26—H, as its interaction angle is 163.0° comparing with 140.5° for the other H-bond.

The cell packing along the *z*-axis is shown in Fig. 3. Each molecule of the dimeric PQC is involved in series of H-bond of different strengths. To clarify this behavior, these molecules are labeled, red (A) and black (B). Both molecules form an own separated infinite chain structure parallel to each other with a trans-zigzag type along "*z*" axis. This happens through formation of intermolecular H-bond with D···A distances, 2.600 Å (N28···H30BO7) and 2.439 Å (O8···H25AC25) for A and B, respectively. In the other words, the trans-zigzag type for "A" molecules is built between C≡N and OCH_3, whereas that of "B" molecules is the contact of C═O and OCH_3. Thus, the keto group in "A" and "B" molecules is not survived in the same environments. This is confirmed by observing two ν(C═O) modes of keto group in the vibrational spectrum. In addition, "A" and "B" molecules interact with each other through H-bond. For example, "A" molecule interacts with three neighboring "B" molecules in the same plane through four H-bonds with different donor acceptor sites (Fig. 3). A big difference is found between "A" and "B" molecules in the packing diagram by observing a π–π stacking only in "A" between the ether ring planes along the crystallographic axis "a" (Fig. 4). It is surprising to find that the standard deviation (SD) between the similar bond lengths (Table 1) in "A" and "B" molecules is 0.042 Å. This means that the two molecules are survived in different environments of H-bond.

3.2. Geometry optimization

Full geometry optimization of dimeric PQC was performed at DFT/B3LYP/6-31G(d) and HF/6-31G(d) level of theory. Monomeric optimization was carried out by HF/6-31G(d). The optimized structures were constructed based on its crystallographic data. The optimized geometry was checked as minima on the potential energy surfaces by frequency calculations. The global energy minimum of dimeric PQC is −3038.271 and −3052.406 Hartree, calculated by HF and DFT, respectively. The energy of the monomeric structure is −1519.131 Hartree. PQC is belonging to C1 symmetry point group. It was found that bond lengths given at DFT/B3LYP level of theory are more accurate than those obtained by HF (Table 1) owing to the inclusion of electron correlation. Most of the optimized bond lengths calculated by DFT are in agreement with the crystal data within |0.000–0.022| Å except O6—C12 (0.029 Å), C9—C24 (0.027 Å), N5—C22 (0.029 Å) and C20—C23 (0.032 Å) bonds. The minor discrepancy may be justified on the basis that the calculations were performed on a single dimeric molecule in the gaseous state contrary to the experimental values, which were recorded in presence of intermolecular interactions. Moreover, the slightly disagreement in O6—C12, C9—C24, N5—C22 and C20—C23 bond distances may be attributed to the participation of "A" molecules in several inter H-bonds as O8···H46—C46, and cyano-methoxyl interactions along the *z*-axis between the similar molecules with a trans-zigzag type (Fig. 3). The largest difference between the experimental ("A" type) and calculated bond lengths is 0.032 Å for DFT/B3LYP and 0.047 Å for HF. Owing to the low scattering factors of hydrogen atoms in X-ray diffraction, the experimental bond lengths of X—H bonds are shorter than the estimated bond lengths.

Moreover, the SD value in the calculated bond lengths for "A" molecules, for example, is 0.019 and 0.021 Å for DFT/B3LYP and HF. A linear fit between the experimental and theoretical bond distances confirms that DFT gives better agreement than HF, and "A"-type molecule structural parameters are more close to the theoretical data than "B"-type.

$d_{calcd} = 0.972d_{exp} + 0.046$ $R^2 = 0.973$ SD = 0.019	DFT/B3LYP ("A" molecule)
$d_{calcd} = 1.024d_{exp} - 0.037$ $R^2 = 0.968$ SD = 0.021	HF ("A" molecule)
$d_{calcd} = 1.020d_{exp} - 0.023$ $R^2 = 0.889$ SD = 0.037	DFT/B3LYP ("B" molecule)
$d_{calcd} = 1.043d_{exp} - 0.063$ $R^2 = 0.837$ SD = 0.046	HF ("B" molecule)

Furthermore, the calculated bond lengths and angles of "A" and "B" molecules, calculated by HF, are the same except O6C12 and N5C24 bonds. These parameters are also consistent with that of the monomeric one at the same level of theory.

3.3. Mulliken atomic charges and molecular electrostatic potential (MEP)

The calculation of effective Mulliken atomic charge plays an important role in the application of quantum mechanical calculations to the molecular systems. As shown in Fig. 5, both C12 (0.363e) and C27 (0.349e) atoms have larger positive charges than the other aromatic carbons. This is due to the attachment of negatively charged $O3CH_3$ and $O6CH_3$. Likewise, C22 atom (0.597e) possesses the maximum positive charge among all carbon atoms in PQC. This is mainly due to attachment of electro-negative oxygen atom (O8). C24 and C29 atoms bear charges of different value and sign, 0.364e and −0.161e, respectively. This is due the withdrawing effect of C≡N on C24 atom. It is confirmed by low charge density on C20 atom (0.068e). It can be seen that the similar atoms in "A" and "B" molecules have nearly the same charge and sign as shown in Fig. 5.

Molecular electrostatic potential (MEP) is related to the electronic density and is a very useful descriptor in understanding sites for electrophilic attack and nucleophilic reactions as well as hydrogen bonding interactions [30]. These maps allow us to visualize variably charged regions of a molecule. Knowledge of the charge distributions can be used to determine how molecules interact with one another. Different values of the electrostatic potential are represented by different colors: red represents regions of most electro negative electrostatic potential, blue represents regions of most positive electrostatic potential and green represents regions of zero potential. Potential increases in the following order: red < orange < yellow < green < blue. Herein, MEP was calculated by B3LYP/6-31G(d) that used for optimization. As shown in Fig. 6, the dimeric PQC has several sites for electrophilic attack, where the negative regions are mainly located over the oxygen atoms of keto (O8: −0.064 a.u.), aldehydic (O37: 0.080 a.u.) and cyano (N33: 0.062 a.u.). These groups are participated in the formation of the variety of H-bond as previously mentioned. In addition, it is interesting to note that the positive regions are localized on hydrogen atoms and especially those of the methoxyl group (C45) apart from cyano group with a maximum value of 0.052 a.u., which can be acted as centers for several inter H-bond with other neighboring molecules.

3.4. Frontier molecular orbitals (FMOs)

FMO's orbitals play an important role in electric and optical properties [31]. HOMO represents the ability to donate an electron, while LUMO represents the ability to accept an electron. The frontier orbital gap helps to characterize the chemical reactivity, optical polarizability and chemical hardness–softness of a molecule. Fig. 7 shows the electron distributions and energy levels of HOMO and LUMO orbitals for the dimeric and monomeric PQC. The HOMO–LUMO energy gap is 3.42 and 7.52 eV for dimeric and monmeric structures, respectively, at the same level of theory. According to Koopman's theorem [32], the ionization energy (I) and electron affinity (A) can be expressed through the energies of HOMO and LUMO as $I = -E_{HOMO}$ and $A = -E_{LUMO}$. Alternatively, the chemical hardness and softness of a molecule are good indicators for the chemical reactivity of a given molecule. From energy gap, one can find whether the molecule is hard or soft. The soft molecule is more polarizable than the hard one because it needs small energy to excitation. Softness (S) is a property of molecule that measures the extent of chemical reactivity. It is defined as the reciprocal of hardness (η) and $\eta = (I - A)/2$ [33]. As shown in Table 3, the dimeric PQC is softer than the monomeric one. In addition, the chemical potential (μ) and electronegativity (χ) of a molecule can be calculated as follows: $\mu = -(I + A)/2$, and $\chi = (I + A)/2$, i.e. $\mu = -\chi$. The chemical potential is found to be −4.24 and −3.75 eV for dimeric and monomeric PQC, respectively. The electrophilicity index (ω), $\omega = \mu^2/2\eta$, [34] is a measure of energy lowering due to maximal electron flow between donor and acceptor. It was found that monomeric PQC acts as a center for nucleophilic activity with a higher electrophilicity index 33.08 eV than its dimeric one, 14.91 eV.

3.5. Electronic spectra

The electronic spectra of isoquinoline-1-acetonitrile **(1)** and 2-hydroxy-9,10-dimethoxy-4-oxo-6,7-dihydro-4*H*-pyrido[2,1-a]isoquinoline-1-carbonitrile **(2)** (Scheme 1) and PQC were reported in ethanol. Two absorption bands at 275 and 320 nm and a shoulder at 255 nm (Fig. 8) are assigned to π–π^* transitions in isoquinoline-1-acetonitrile. For compound **(2)**, these bands are

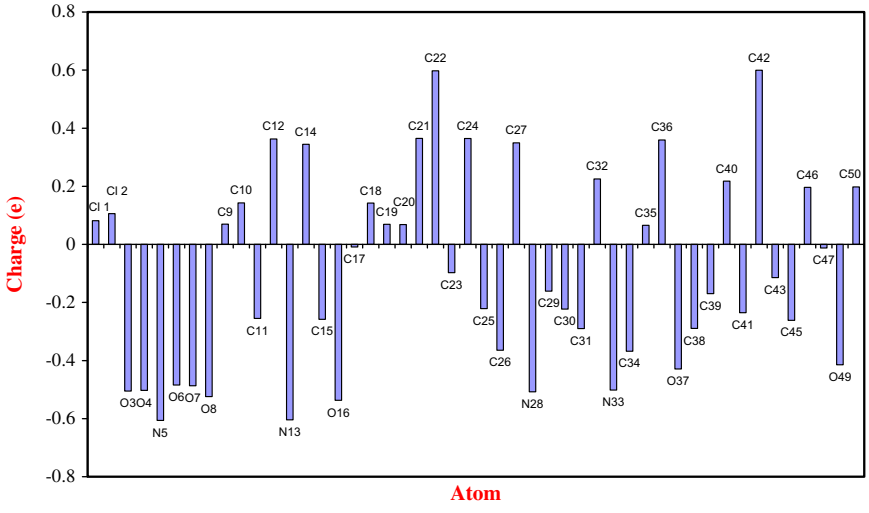

Fig. 5. Mulliken charges of PQC calculated at DFT/B3LYP/6-31G(d) level of theory.

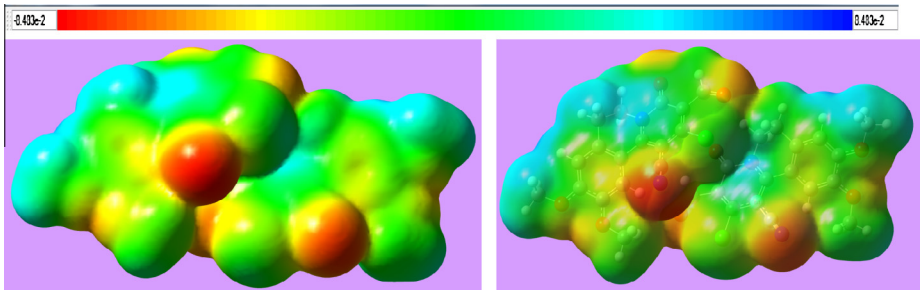

Fig. 6. Molecular electrostatic potential map calculated at DFT/B3LYP level of PQC. The electron density isosurface is 0.004 a.u.

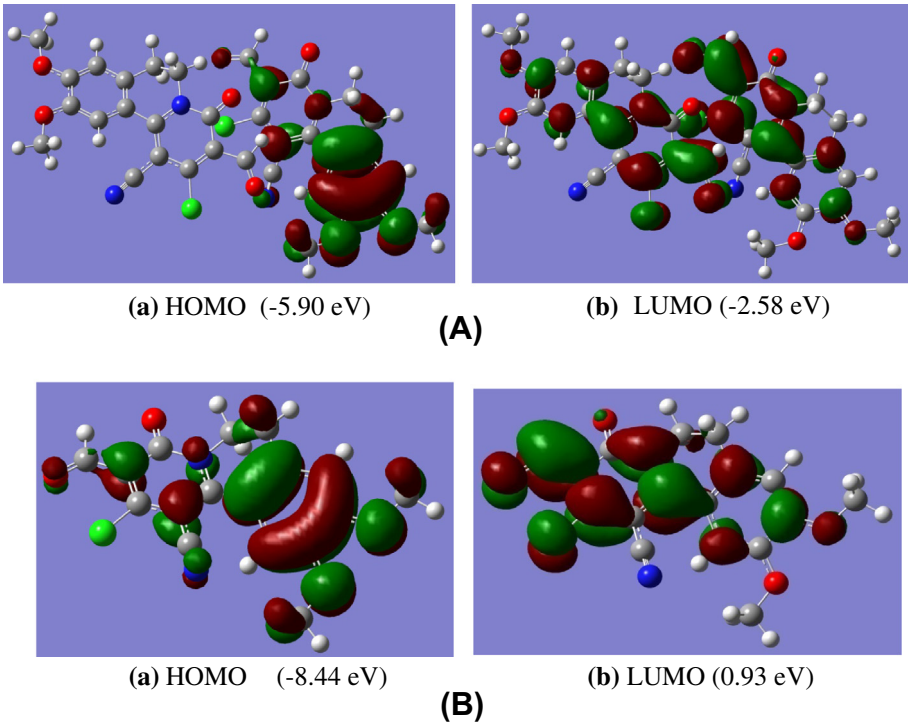

Fig. 7. Molecular orbital surfaces of (A) dimeric and (B) monomeric PQC.

Table 3
Quantum chemical descriptors based on HF calculations for dimeric and monomeric PQC.

Quantum parameter	Dimer	Monomer
Total energy (a.u.)	−3052.41	−1519.13
E_{HOMO} (eV)	−5.90	−8.44
E_{LUMO} (eV)	−2.58	0.93
ΔE_{gap} (eV)	3.42	7.52
Ionization energy (I)	5.90	8.44
Electron affinity (A)	2.58	0.93
Mulliken electronegativity (χ)	4.24	3.75
Softness (S)	0.60	0.21
Hardness (η)	1.65	4.68
Electrophilicity index (ω)	14.91	33.08

slightly red shifted to 260, 275 and 330 nm due to the hyperconjugative effect of the attached substituents. PQC spectrum showed three absorption bands at 260, 285 and 380 nm and a shoulder at 400 nm. The broad longer wavelength band at 380 nm can be assigned to an intramolecular charge transfer interaction from the aromatic nucleus to the neighboring cyano acceptor center [10].

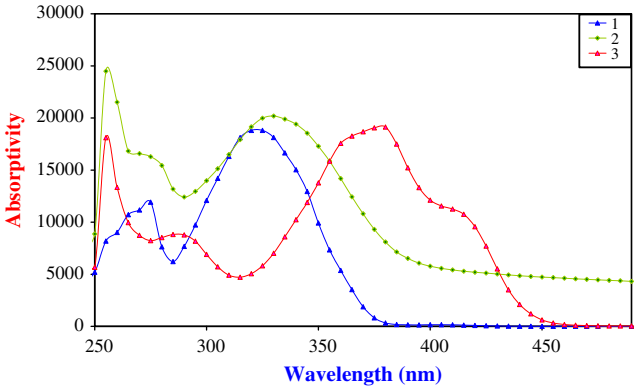

Fig. 8. Experimental electronic absorption spectra of (1) isoquinoline-1-acetonitrile, (2) 2-hydroxy-9,10-dimethoxy-4-oxo-6,7-dihydro-4*H*-pyrido[2,1-*a*]isoquinoline-1-carbonitrile and (3) PQC in ethanol.

The nature of the electronic transitions observed in the UV–Vis. spectra of PQC in the gaseous state, ethanol and DMF has been studied by TD-DFT. The lowest 20 spin-allowed excitation states

were taken into consideration for calculation of its electronic absorption spectra. The absorption spectra were simulated using *GAUSSSUM* [35]. The calculated energies of excitation states with transition strength ($f > 0.001$) are tabulated (Supplementary material, Table S2). The primary feature of TD-DFT spectrum of PQC in gaseous state shows mainly four absorption bands at 225, 249, 295 and 398 nm with oscillator strength 0.0871, 0.1646, 0.0793 and 0.327 respectively. The lowest energy absorption band at 398 nm predominately arises from transition of HOMO to LUMO (95%). The excitation energy at 295 nm (4.19 eV) is contributed mainly from HOMO → LUMO+1 transition with configuration interaction coefficient up to 0.72. The sharp band at 249 nm is assigned to a combination of HOMO−5 → LUMO (43%) and HOMO−2 → LUMO+1 (29%). The highest energy transition at 225 nm characterizes mainly the transitions HOMO−7 → LUMO (47%) and HOMO−2 → LUMO+2 (38%). On the other hand, the theoretical UV–Vis. spectra of PQC in ethanol and DMF are typical, but different from the gaseous state with five bands at 219, 239, 313, 362 and 426 as well as a shoulder at 271 nm. The lowest energy electronic transition (HOMO → LUMO) (Fig. 9) in ethanol is red shifted to 426 nm (2.91 eV) with respect to the gaseous state. The band appears as a shoulder in the gaseous state is now located at 362 nm and assigned to HOMO−1 → LUMO (97%). Moreover, the excitation energy at 313 nm is attributed to HOMO → LUMO+1 (58%) and HOMO−3 → LUMO (38%). The shoulder at 271 nm is coming from HOMO−1 → LUMO+1 (56%) and HOMO−2 → LUMO+1 (21%) transitions, while the band energy transition at 239 nm is assigned to HOMO−3 → LUMO+1 (40%), HOMO → LUMO+3 (25%). The highest band at 219 nm ($f = 0.2264$) is attributed to HOMO−1 → LUMO+2 (62%) transition.

3.6. Natural bond orbital (NBO) analysis

NBO approach [26] has been frequently used in evaluation of intra- and intermolecular interactions, and provides a convenient basis for investigating charge transfer or conjugative interaction in molecular systems. NBO analysis was performed to provide the contribution of atomic orbitals to NBO σ and π hybrid orbitals for bonded atom pairs. Three NBO hybrid orbitals are defined, bonding orbital (BO), lone pair (LP) and core (CR). The ideal Lewis structure picture is constructed from Lewis σ-type (donor) NBOs that are complemented by non-Lewis σ-type (acceptor) NBOs. The filled NBOs describe covalency effects in molecules, while the anti-bonds represent empty valence-shell capacity and spanning portions of the atomic valence space that are formally unsaturated by covalent electrons. Weak occupancies of the valence anti-bonds signal irreducible departure from an idealized localized Lewis picture, i.e. true "delocalization effects". Hyperconjugation is given as a stabilizing effect and arises from an overlap between an occupied and another electron deficient orbital. Hyperconjugative interaction energy was deduced from the second-order perturbation approach of Fock matrix in NBO basis between donor–acceptor orbitals [36]. The larger the second order interaction energy (E^2) value, the more intensive is the interaction between electron donors and electron acceptors, i.e. the more donating tendency from electron donors to electron acceptors and the greater the extent of conjugation of the whole system. These interactions can be identified by finding an increase in the electron density (ED) of the anti-bonding orbital that weakens the respective bonds.

NBO analysis of "A" molecules, as a representative example, in the dimeric PQC shows that π(C12—C38) and π(C15—C27) participate as donors and π^*(C9—C10) as an acceptor with charge transfer energy values ~23 and 17 kcal mol^{-1}, respectively. These interactions weaken and elongate C9—C10 bond (1.405 Å) as calculated by DFT. Other π electrons intramolecular interactions are found in the aromatic moiety revealing delocalization of π electrons. NBO reveals that σ(C9—C10) is formed from $sp^{1.91}$ hybrid on C9 (65.56% p) and $sp^{1.99}$ on C10 (66.57% p). LP(1)N5 → π^*(O8—C22) (ED ≈ 0.354e and E^2 = 47 kcal mol^{-1}) interaction has a small energy difference (~0.28 a.u.) supporting electron delocalization between isoquinoline nitrogen and C=O (keto). This leads to an improvement in the coordination ability of PQC *via* keto group. Furthermore, the ligational behavior of C=O (keto) has been supported by π(C17—C23) → π^*(O8—C22) (E^2 = 26.42 kcal mol^{-1}) interaction. LP(3)Cl 1 → π^*(C17—C23) (ED ≈ 0.031e and E^2 = 16.84 kcal mol^{-1}) is responsible for conjugation between C17—C23 bond and aldehydic group (C46=O37). The strongest hyper-interaction in PQC is coming from LP(1)N5 → π^*(C20—C24) charge transfer (Table 4), but this has been compensated by the electron withdrawing effect of C≡N and appears of a positive charge upon C24 as previously mentioned. It can be seen that O8—C22 bond (σ(O8—C22) = 0.805 $sp^{1.43}d^{0.01}$ + 0.594 $sp^{2.07}$) is longer than O20—C46 bond (σ(O20—C46) = 0.811 $sp^{1.41}d^{0.01}$ + 0.585 $sp^{2.18}$). The slightly increasing in p character of C46 relative to C22 atom leads to different bond distances for the two C=O groups. NBO analysis has been also performed to throw more light on the intermolecular interactions between "A" and "B" molecules. Two H-bonds were found as previously mentioned, LP(2)Cl 1 → σ^*(C26—H) (E^2 = 80 cal mol^{-1}) and LP(2)O45 → σ^*(C45—H) (E^2 = 1530 cal mol^{-1}). These interactions lead to an increase in electron density (ED) of σ^*(C26—H) (0.017e) and σ^*(C45—H) (0.023e), respectively.

3.7. IR assignment

The calculation of the vibrational frequencies is a very useful task for assignment of the spectra. The vibrational frequencies obtained by quantum chemical calculations are usually higher than the corresponding experimental quantities owing to several factors such as anharmonicity and basis set deficiencies [21,22]. Scale factors were introduced [24–26] to overcome these shortcomings. Herein, uniform scaling method is introduced, where vibrational frequencies are scaled as 0.958 for B3LYP/6-31G(d) for the range of wavenumbers above 1700 cm^{-1}, and 0.983 for those below 1700 cm^{-1}, as well as 0.9067 for HF/6-31G(d) (Supplementary material, Table S3)

Generally, aromatic compounds exhibit multiple weak bands in the region 3100–3000 cm^{-1} due to the aromatic C—H stretching modes. Theoretically, dimeric PQC gives rise to four C—H aromatic stretching modes of vibration related to presence of four aromatic C—H bonds. These vibration modes are allocated at 3148, 3144, 3088 and 3085 cm^{-1} as calculated at DFT/B3LYP level of theory. For assignments of CH_3 group frequencies theoretically, nine fundamentals can be associated to each CH_3 group [37]. The scaled bands at 3038 and 2990 cm^{-1} are ascribed to CH_3 (C45) asymmetric mode, while that at 2917 cm^{-1} is attributed to its $\nu_{ss}(CH_3)$. Similar, the bands at 3037, 2970; and 2908 are assigned to $\nu_{ass}(CH_3)$ and $\nu_{ss}(CH_3)$ for C30. Infrared bands established at 1519, 1503, 1483, 1206, 1163, and 286 cm^{-1} are allocated to CH_3^{opb}, CH_3^{ipb}, CH_3^{sb}, CH_3^{opr}, CH_3^{ipr}, and τCH_3 (C45) vibration mode, respectively. These vibrations are established at 1504, 1496, 1480, 1201, 1162, and 280 cm^{-1}, for methyl group No. 30, respectively. On the same approach, six fundamentals [22] can be associated to each CH_2 group in the studied compound. For example, the bands observed at 3081, and 2936 cm^{-1} are ascribed to CH_2 (C39) asymmetric and symmetric stretching vibration. Moreover, infrared bands established at 1507, 1359, 1254, and 1066 cm^{-1} are attributed to $\delta_s CH_2$, ωCH_2, τCH_2, and ρCH_2 vibration modes, respectively.

The aromatic carbon–carbon stretching vibrations occur in the region 1625–1430 cm^{-1}. These bands are of variable intensities and are observed at 1625–1590, 1590–1575, 1540–1470, 1465–1430 and 1380–1280 cm^{-1} from the frequency ranges given by

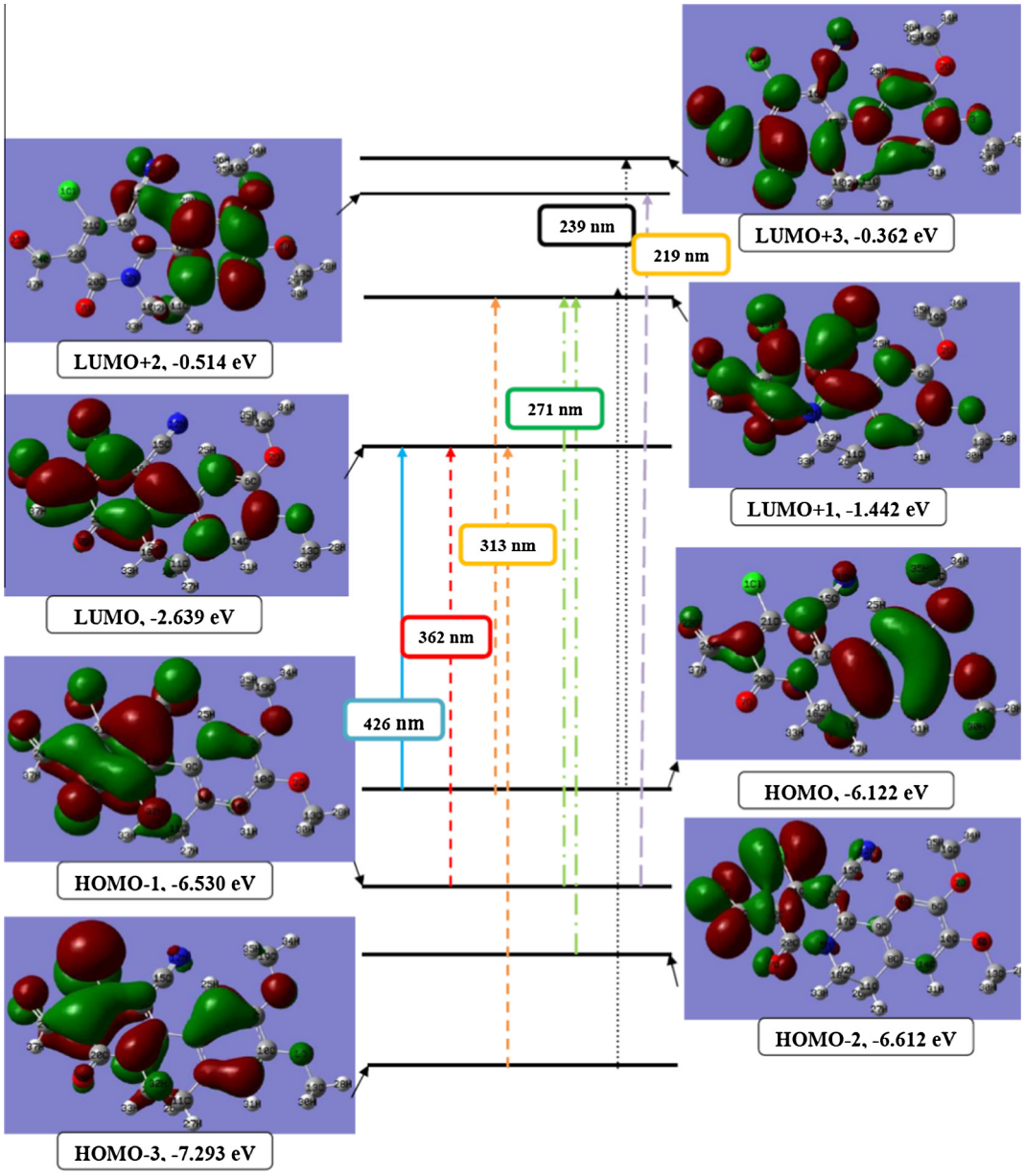

Fig. 9. Theoretical electronic absorption transitions for PQC in ethanol.

Varsanyi [38] for the five bands in the region. The actual positions of these bands are not determined so much by the nature of the substituents, but with the form of the substitution around the ring [39]. However, mono and disubstituted benzenes absorb near 1600, 1580, 1500 and 1450 cm^{-1}. The characteristic skeletal vibration modes of the titled dimeric compound show two bands at 1585 and 1462 cm^{-1}. The DFT calculations predict a group of C=C stretching vibrations near 1629 and 1424 cm^{-1} due to the benzene moiety and their wavenumbers are found very close to the observed values as shown (Supplementary material, Table S3). It can be seen also that the scaled aromatic bands, calculated by HF, estimate higher than those calculated by DFT.

Experimentally, the sharp band at 2214 cm^{-1} is assigned to ν(C≡N) with deviation of 22 cm^{-1} from the theoretically scaled value given by DFT. The slightly discrepancy may be justified on the basis that the calculations were performed on a single molecule in the gaseous state contrary to the experimental values, which were recorded in presence of intermolecular interactions, where the cyano group is participated in a H-bond as previously mentioned in X-ray part. It was found that HF estimates higher than DFT with deviation of 100 cm^{-1} from the experimental value. Moreover, the introduction of a carbonyl group conjugated to a C=C bond results in the delocalization of the π-electrons in the C=O and C=C bonds. This conjugation increases the single bond characters of C=O and C=C bonds in the resonance hybrid and hence lowers their force constants. This can justify the assignment of ν(C=C) modes of isoquinoline at 1608 and 1546 cm^{-1}. The band at 1720 cm^{-1} is allocated to the aldehydic group with deviation of 19 cm^{-1} due to involvement of this group in intra-molecular H-bond with keto group and another H-bond with methoxyl groups. HF is still away from the agreement with the experimental data. The two bands at 1697 and 1651 cm^{-1} are assigned to the keto group in a dimeric PQC, since this group is not in the same environments in the two molecules. The former band is assigned to keto group in red molecules, while the lower wavenumber band is attributed to keto group in black molecules (Fig. 3). The theoreti-

Table 4
Second order perturbation theory analysis of Fock matrix in NBO basis (selected).

Molecule A					Molecule B				
Donor (*i*)	Acceptor (*j*)	E^2 (kcal/mol)	$E(j)-E(i)$ a.u.	$F(i,j)$ a.u.	Donor (*i*)	Acceptor (*j*)	E^2 (kcal/mol)	$E(j)-E(i)$ a.u.	$F(i,j)$ a.u.
π(C12—C38)	π*(C9—C10)	22.95	0.29	0.075	π(C21—C31)	π*(C18—C19)	23.27	0.30	0.076
π(C12—C38)	π*(C15—C27)	15.55	0.30	0.061	π(C21—C31)	π*(C11—C14)	15.84	0.30	0.061
π(C15—C27)	π*(C9—C10)	16.99	0.29	0.065	π(C11—C14)	π*(C18—C19)	16.15	0.29	0.064
π(C17—C23)	π*(O8—C22)	26.42	0.29	0.080	π(C43—C47)	π*(O16—C42)	18.81	0.30	0.070
π(C17—C23)	π*(O37—C46)	18.56	0.30	0.069	π(C43—C47)	π*(O49—C50)	18.81	0.30	0.070
π(C20—C24)	π*(C17—C23)	25.89	0.28	0.077	π(C35—C36)	π*(C43—C47)	25.78	0.28	0.077
π(C20—C24)	π*(N33—C40)	20.75	0.39	0.085	π(C35—C36)	π*(N28—C32)	20.82	0.38	0.085
LP(3)Cl 1	π*(C17—C23)	16.84	0.33	0.070	LP(3)Cl 2	π*(C43—C47)	17.63	0.32	0.071
LP(2)O3	π*(C15—C27)	34.22	0.33	0.099	LP(2)O7	π*(C21—C31)	34.39	0.34	0.101
LP(1)N5	π*(O8—C22)	47.02	0.28	0.105					
LP(1)N5	π*(C20—C24)	57.01	0.27	0.113	LP(1)N13	π* (C35—C36)	57.87	0.27	0.113
LP(2)O6	π*(C12—C38)	34.43	0.34	0.101	LP(2)O4	π*(C11—C14)	32.36	0.33	0.097
LP(2)O8	π*(N5—C22)	29.70	0.63	0.123	LP(2)O16	π*(N13—C42)	29.19	0.63	0.123
LP(2)O8	π*(C17—C22)	17.77	0.72	0.103	LP(2)O16	π*(C42—C47)	17.52	0.72	0.103
LP(1)N33	π*(C20—C40)	13.35	1.02	0.104	LP(1)N28	π*(C32—C35)	13.28	1.02	0.104
LP(2)O37	σ*(C17—C46)	20.51	0.71	0.109	LP(2)O49	π*(C47—C50)	21.12	0.71	0.110
LP(2)Cl 1	σ*(C26—H)	0.08	0.77	0.007	LP(2)O49	σ*(C45—H)	1.53	0.73	0.031
LP(2)O37	σ*(C39—H)	0.10	0.75	0.008	LP(3)O16	π*(C17—C23)	0.17	0.24	0.006
LP(1)O37	σ*(C18—C26)	0.10	1.11	0.009					
LP(2)O45	σ*(C45—H45)	1.53	0.73	0.031					

cally scaled bands at 1676 and 1666 cm^{-1}, calculated by DFT/B3LYP are assigned to ν(C=O) of keto groups. This discrepancy between the experimental and theoretical modes is due to negligence of the intermolecular interactions in our calculations.

3.7.1. ^1H NMR spectral analysis

In order to provide an unambiguous assignment of ^1H NMR spectrum of the monomeric PQC, we undertook a series of NMR calculations at DFT/B3LYP/6-311 + G(2d,p) level of theory by applying GIAO approach [24]. The values for the ^1H isotropic were referenced to TMS, which was calculated at the same level of theory. The default PCM model provided by Gaussain03 was also tested in order to describe the influence exerted by solvent (DMSO) on the NMR spectrum of the given compound. First, it is worthy to mention that the H atom is the smallest of all atoms and mostly localized on the periphery of molecules. Thus, the chemical shifts will be more susceptible to inter- and intramolecular interactions in the aqueous solution comparing with those for other heavier atoms. Another important aspect is that, hydrogen attached or nearby electron-withdrawing atom or group can decrease the shielding and moves the resonance of attached proton towards a higher frequency. By contrast, electron donating atom or group increases the shielding and moves the resonance towards a lower frequency. As shown in Table 5, the ^1H chemical shifts of all protons in the investigated compound, except the aldehydic proton (H_{46}), are in a good agreement with those theoretically calculated by the PCM model. The regression coefficient between the calculated and the experimental chemical shifts is improved in presence of DMSO as a solvent. The aldehydic proton (H_{46}) is found at 10.14 ppm and is shifted towards a higher magnetic field than the calculated one by 0.81 ppm in case of DMSO and 0.94 ppm in the gaseous state as calculated by DFT/B3LYP/6-311 + G(2d,p) [40]. Although, the chemical shift of aldehydic proton in DMSO shows little improvement in relation to the gaseous state, but this value remains slightly unacceptable apart from the experimental value, which can reflect that the chemical shift associated with this proton is not correctly described by continuum model. Thus, it is clear that PCM model fails, to some extent, in reproducing the experimental findings for the hydrogen-bonded protons and specific solute–solvent interactions are expected to completely explain the NMR spectra of the studied compound [24].

Table 5
Experimental and calculated ^1H NMR chemical shifts for titled monomeric PQC.

Atom	δ Calcd.		δ Exp.
	Gaseous	DMSO	DMSO
H_{15}	8.44	8.32	7.89
H_{25}	4.08	4.03	3.84
H_{29}	4.22	4.29	4.11
H_{34}	2.78	3.00	2.98
H_{38}	6.74	7.14	7.15
H_{45}	4.02	4.07	3.91
H_{46}	11.08	10.95	10.14
R^2	0.9825	0.9951	

3.8. Anticancer activity

To evaluate the potential usefulness of the titled compound synthesized as antitumor agent, three cell lines of different origin *breast cancer* (MCF7), *colon Carcinoma* (HCT) and *human hepatocarcinoma* ($HepG_2$) were treated. The IC_{50} (the concentration that inhibited in 50% of the cellular proliferation) of studied compound and Doxorubicin were determined (Fig. 10). According to Shier [41], the compounds exhibited IC_{50} activity within the range of 10–25 μg/ml are considered weak anticancer drugs, while those

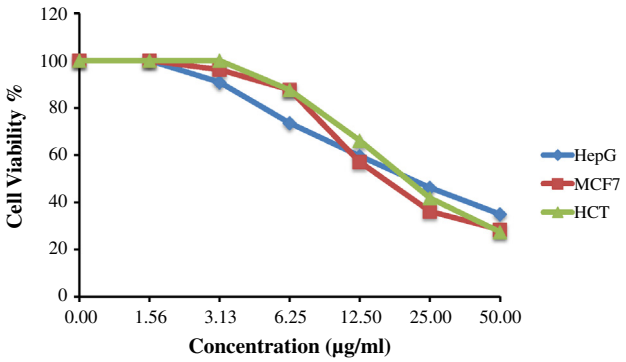

Fig. 10. The effect of concentration (μg/ml) of PQC on inhibition of MCF7, HCT and $HEPG_2$.

of IC_{50} activity between 5 and 10 μg/ml are moderate and compounds of activity below 5 μg/ml are considered strong agents. The determined IC_{50} values for Doxorubicin, against the studied cell lines, are 0.469, 1.20 and 2.38 μg/ml for HCT, $HEPG_2$, and MCF7, respectively. Alternatively, it can be seen that the titled compound is toxic against the cell lines but less than Doxorubicin. In general, with the lower IC_{50} value obtained for PQC against MCF7 cells in comparable with other cell lines, it can be concluded that MCF7 cell line is more sensitive to this compound than the other cell lines. The IC_{50} values of PQC against MCF7, HCT and $HepG_2$ are found to be 16.7, 20.8 and 21.4 μg, respectively. Thus, according to Shier scale, the titled compound shows weak antitumor activity compared with Doxorubicin.

4. Conclusion

In an effort to prepare new compounds with potential biological activity, we have synthesized and characterized 2-chloro-3-formyl-9,10-dimethoxy-4-oxo-6,7-dihydro-4H-pyrido[2,1-a]isoquinoline-1-carbonitrile (PQC) by different physico-chemical techniques. The unit cell of PQC is built by two molecules that have different structural parameters. The experimental studies were complemented by quantum chemical calculations at DFT and HF level of theory. The reasonable agreement between the theoretical and experimental data reflects, to great extent, the suitability of the applied method for this type of work. The inclusion of solvation parameter to NMR calculations proved to be very important in obtaining better values than in gaseous state, and especially for acidic protons. PQC has several sites for electrophilic attack like C≡N and C═O. Monomeric PQC acts as a center for nucleophilic activity with a high electrophilicity index than its dimeric one. The cytotoxicity assay revealed that MCF7 cell line is more sensitive to PQC than the other studied cell lines.

Appendix A. Supplementary material

Supplementary data associated with this article can be found, in the online version, at http://dx.doi.org/10.1016/j.molstruc.2013.04.032.

References

[1] M. Kidwai, K.R. Bhushan, P. Sapra, R.K. Saxena, R. Gupta, Bioorg. Med. Chem. Lett. 8 (2000) 69.
[2] L. Strekowski, J.L. Mokrosz, V.A. Honkan, A. Czarxy, M.T. Ceyla, R.L. Wydra, S.E. Patterson, R.F. Schinazi, J. Med. Chem. 34 (1991) 1739.
[3] P.G. Bray, S.R. Hawley, S.A. Ward, Mol. Pharmacol. 50 (1996) 1551.
[4] A. Sparatore, N. Basilico, M. Casagrande, S. Parapini, D. Taramelli, R. Brun, S. Wittlin, F. Sparatore, Bioorg. Med. Chem. Lett. 18 (2008) 3737.
[5] A.W. Sweeney, C.R.B. Blackburn, K.H. Rieckmann, Am. J. Trop. Med. Hyg. 71 (2004) 187.
[6] S. Tiwari, P.M.S. Chauhan, A.P. Bhaduri, N. Fatima, R.K. Chatterjee, Bioorg. Med. Chem. Lett. 10 (2000) 1409.
[7] L.W. Deady, J. Desneres, A.J. Kaye, G.J. Finlay, B.C. Baguley, W.A. Denny, Bioorg. Med. Chem. 9 (2001) 445.
[8] K.M. Khan, Z.S. Zaify, Z.A. Khan, Drug Res. 50 (2000) 915.
[9] N.T. Abdel-Ghani, A.M. Mansour, Eur. J. Med. Chem. 47 (2012) 399–411.
[10] N.T. Abdel-Ghani, A.M. Mansour, Inorg. Chim. Acta 373 (2011) 249–258.
[11] A.M. Mansour, Inorg. Chim. Acta 394 (2013) 436–445.
[12] H.T. Openshau, N. Whittaker, J. Chem. Soc. (1961) 4939.
[13] T. Kappe, Y. Linnau, Monats. Chem. 100 (1969) 1726.
[14] H.M. Hassaneen, W.W. Wardkhan, Y.Sh. Mohammed, Heterocycles 85 (12) (2012) 2933–2947.
[15] A.L. Spek, J. Appl. Cryst. 36 (2003) 7–13.
[16] A.L. Spek, Program for Reduction of CAD-4 Data, University of Utrecht, The Netherlands, 1996.
[17] A. Altomare, G. Cascarano, C. Giacovazzo, A. Guagliardi, M.C. Burla, G. Polidori, M. Camalli, J. Appl. Cryst. 27 (1994) 435–436.
[18] S. Mackay, C.J. Gilmore, C. Edwards, N. Stewart, K. Shankland, Maxus computer program for the solution and refinement of crystal structures, Bruker Nonius, The Netherlands, MacScience, Japan & The University of Glasgow, 1999.
[19] C.K. Johnson, ORTEP-II. A Fortran Thermal-Ellipsoid Plot Program. Report ORNL-5138, Oak Ridge National Laboratory, Oak Ridge, Tennessee, USA, 1976.
[20] M.J. Frisch, G.W. Trucks, H.B. Schlegel, G.E. Scuseria, M.A. Robb, J.R. Cheeseman, V.G. Zakrzewski, J.A. Montgomery, R.E. Stratmann, J.C. Burant, S. Dapprich, J.M. Millam, A.D. Daniels, K.N. Kudin, M.C. Strain, O. Farkas, J. Tomasi, V. Barone, M. Cossi, R. Cammi, B. Mennucci, C. Pomelli, C. Adamo, S. Clifford, J. Ochterski, G.A. Petersson, P.Y. Ayala, Q. Cui, K. Morokuma, D.K. Malick, A.D. Rabuck, K. Raghavachari, J.B. Foresman, J. Cioslowski, J.V. Ortiz, A.G. Baboul, B.B. Stefanov, G. Liu, A. Liashenko, P. Piskorz, I. Komaromi, R. Gomperts, R.L. Martin, D.J. Fox, T. Keith, M.A. Al-Laham, C.Y. Peng, A. Nanayakkara, C. Gonzalez, M. Challacombe, P.M.W. Gill, B.G. Johnson, W. Chen, M.W. Wong, J.L. Andres, M. Head-Gordon, E.S. Replogle, J.A. Pople, GAUSSIAN 03 (Revision A.9), Gaussian, Inc., Pittsburgh, 2003.
[21] A. Frisch, A.B. Nielson, A.J. Holder, GAUSSVIEW User Manual, Gaussian Inc, Pittsburgh, PA, 2000.
[22] N.T. Abdel-Ghani, A.M. Mansour, Spectrochim. Acta A 81 (2011) 529–543.
[23] N.T. Abdel-Ghani, A.M. Mansour, Spectrochim. Acta A 86 (2012) 605–613.
[24] M. Karabacak, M. Kurt, Spectrochim. Acta A 71 (2008) 876–883.
[25] N.T. Abdel-Ghani, A.M. Mansour, Spectrochim. Acta A 91 (2012) 272–284.
[26] N.T. Abdel-Ghani, M.F. Abo El-Ghar, A.M. Mansour, Spectrochim. Acta A 104 (2013) 134–142.
[27] N.T. Abdel-Ghani, A.M. Mansour, J. Coord. Chem. 65 (5) (2012) 763–779.
[28] P. Skehan, R. Smreng, D. Scudiero, A. Monks, J. McMahon, D. Vistica, J.T. Warren, H. Bokesch, S. Kenney, M.R. Boyd, J. Nat. Cancer Inst. 82 (1990) 107–1112;
A. Monks, D. Scudiero, P. Skehan, K. Paull, D. Vistica, C. Hose, J. Langley, P. Cronise, A. Viagro-Wolff, M. Gra-Goodrich, J. Nat. Cancer Inst. 83 (1991) 757–766.
[29] C.M. Lozano, O. Cox, M.M. Muir, J.D. Morales, J.L. Rodríguez-Cabáin, P.E. Vivas-Mejfa, F.A. Gonzalez, Inorg. Chim. Acta 271 (1998) 137–144.
[30] S. Güveli, N. Özdemir, T. Bal-Demirci, B. Ülküseven, M. Dinçer, Ö. Andaç, Polyhedron 29 (2010) 2393–2403.
[31] I. Fleming, Frontier Orbitals and Organic Chemical Reactions, Wiley, London, 1976.
[32] T.A. Koopmans, Physica 1 (1933) 104.
[33] H. Chermette, J. Comp. Chem. 20 (1999) 129–154.
[34] R.G. Parr, W. Yang, J. Am. Chem. Soc. 106 (1984) 4049.
[35] N.M. O'Boyle, A.L. Tenderholt, K.M. Langner, J. Comp. Chem. 29 (2008) 839.
[36] C. Ravikumar, I. Hubert Joe, V.S. Jayakumar, Chem. Phys. Lett. 460 (2008) 552–558.
[37] N.T. Abdel-Ghani, A.M. Mansour, Spectrochim. Acta A 81 (2011) 754–763.
[38] G. Varsanyi, Vibrational Spectra of Benzene Derivatives, Academic Press, New York, 1969.
[39] D.L. Pavia, G.M. Lampman, G.S. Kriz, Introduction to Spectroscopy, Second ed., Saunders College Publishing, 1996.
[40] N.T. Abdel-Ghani, A.M. Mansour, J. Mol. Struct. 991 (2011) 108–126.
[41] W.T. Shier, Mammalian Cell Culture on $5 a Day: A Lab Manual of Low Cost Methods, University of the Philippines, Los Banos, 1991. p. 64.